Journal of Power Sources 262 (2014) 44–49

Contents lists available at ScienceDirect

Journal of Power Sources

journal homepage: www.elsevier.com/locate/jpowsour

High-performance porous electrodes for pseudosupercapacitors based on graphene-beaded carbon nanofibers surface-coated with nanostructured conducting polymers

Zhengping Zhou, Xiang-Fa Wu*

Department of Mechanical Engineering, North Dakota State University, Fargo, ND 58108, USA

HIGHLIGHTS

- Graphene-beaded carbon nanofibers coated with polyaniline were synthesized.
- Pseudosupercapacitor electrodes based on novel nanofibrous electrodes were fabricated.
- Microstructures and electrochemical properties of the electrodes were tested.
- Improved electrochemical performance of the new nanofibrous electrodes was observed.
- Mechanisms responsible for the improved performance were explored.

GRAPHICAL ABSTRACT

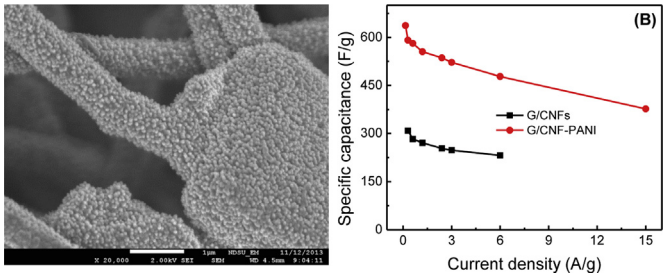

ARTICLE INFO

Article history:
Received 18 December 2013
Received in revised form
18 March 2014
Accepted 20 March 2014
Available online 27 March 2014

Keywords:
Pseudosupercapacitor
Carbon nanofibers
Conducting polymer
Electrospinning
Electrode materials

ABSTRACT

This paper reports the fabrication and electrochemical properties of novel high-performance pseudosupercapacitor electrodes made of graphene-beaded carbon nanofibers (G/CNFs) surface-coated with nanostructured conducting polymers. The G/CNFs were produced by electrospinning the precursor graphene-beaded polymer nanofibers, followed by controlled pyrolysis. *In situ* polymerization in aqueous solution was utilized to coat an ultrathin layer of thorn-like polyaniline (PANI) nanorods onto the G/CNFs to form ternary PANI-coated G/CNFs (PANI-G/CNFs). The highly porous network morphology of PANI-G/CNFs exhibited a very large specific surface area, low internal resistance, and fast redox rate. Electrochemical characterization indicated that the PANI-G/CNF based pseudosupercapacitors carried a high value of specific capacitance up to 637 F g^{-1} at a current density of 0.15 A g^{-1} and still maintained the high value of specific capacitance of 478 F g^{-1} (only 25% decrease) even at a high current density of 6 A g^{-1}. The pseudosupercapacitor showed a very good cycling stability of 87% after 1000 charge/discharge cycles at a very high current density of 15 A g^{-1}. The experimental results indicated that the novel hierarchical, porous PANI-G/CNFs are a promising electrode material for use in high-performance energy storage devices.

1. Introduction

Graphene consists of two-dimensional (2D) monolayers of sp^2-bonded carbon atoms and has attracted extensive attention in the last decade [1–6]. Graphene exhibits unique physical and chemical

* Corresponding author.
E-mail address: Xiangfa.Wu@ndsu.edu (X.-F. Wu).

http://dx.doi.org/10.1016/j.jpowsour.2014.03.096
0378-7753/

properties including excellent electrical conductivity ($\sim 2 \times 10^3$ S cm^{-1}) [7], very large specific surface area (~ 3100 m^2 g^{-1}) [8], and amazing intrinsic electron mobility ($\sim 200{,}000$ cm^2 V^{-1} s^{-1}) [9]. These unique features make graphene a promising nanostructured material for broad applications in microelectronics, energy storage devices, fuel cells, sensors, and gas sorbents, among others [10–12]. In particular, graphene-based materials can be used as high-performance electrodes for electrochemical double-layer capacitors (EDLCs) and pseudocapacitors, which have demonstrated higher values of specific capacitance than other carbonaceous materials, *e.g.*, carbon nanotubes (CNTs), carbon nanofibers (CNFs), and activated carbon [10–13]. Graphene can also be conveniently manufactured in large quantity at low cost from graphite by means of chemical exfoliation [14]. Furthermore, recent intensive investigations have pointed out that metal oxides (*e.g.*, RuO_2, MnO_2, etc.) or conducting polymers (*e.g.*, polyaniline (PANI), polythiophene, polypyrrole, etc.) doped onto the surface of graphene nanosheets can noticeably enhance the electrochemical performance of the resulting supercapacitors with graphene as electrodes [15–18]. Among a variety of conducting polymers, PANI has been under intensive investigation due to its high specific capacitance (up to 750 F g^{-1}), low cost, easy synthesis, and favorable environmental stability [15]. However, several outstanding issues (*e.g.*, the redox switching, low electrical conductivity and poor cyclability) influence the pseudocapacitive performance of PANI when structured as electrode material of supercapacitors [16]. These issues need to be resolved in rendering PANI as a highly effective electrode material to meet the practical requirements of supercapacitors.

It has been reported that graphene nanosheets surface-coated with nanostructured PANI (*e.g.*, nanotubes, nanorods or nanospheres) have demonstrated improved capacitive performance compared to other carbonaceous counterparts and pure PANI [17–21]. Yet, most graphene/PANI electrode materials reported in the literature are in the powder form. Such generic discrete structure requires conductive additives and binders (*e.g.*, polyvinylidene difluoride (PVDF)) to bind the active material and the electrode to the current collector in the process of supercapacitor fabrication. In addition, the effective electrochemical performance of a supercapacitor is limited by the restacking and aggregation of graphene nanosheets, which typically results in irreversible agglomeration and folding/scrolling [13]. Recently, we reported a unique route to synthesize innovative graphene-beaded CNFs (G/CNFs) for use as porous electrode material, in which the synthesis relies on the top-down electrospinning technique followed by controlled pyrolysis and activation [22]. In such a process, graphene nanosheets were covalently connected to the CNFs. Such unique carboneous nanostructures can provide very large specific surface area and high electrical conductivity, which can effectively suppress the restacking and aggregation of graphene nanosheets and meanwhile eliminates the need of conductive binder typically used for electrodes. In addition, porous G/CNF films can be directly utilized as supercapacitor electrodes with high specific capacitance.

In this work, a new technical route is devised to introduce the unique pseudocapacitive effect of G/CNF-based electrode materials via coating an ultrathin layer of thorn-like PANI nanorods onto G/CNFs to form a ternary multifunctional electrode material: PANI-coated G/CNFs (PANI-G/CNFs). Such porous, multifunctional PANI-G/CNF films carry superior intrinsic connectivity and very high specific surface area due to the formation of thorn-like PANI nanorods on the graphene nanosheets and backbone CNFs. Field-emission scanning electron microscopy (FE-SEM) was employed to characterize the unique morphology and microstructure of the G/CNFs and PANI-G/CNFs. The electrochemical behavior of the novel porous electrode materials was characterized in 1 M H_2SO_4 aqueous solution based on a two-electrode cell that was made of a pair of electrodes of 1.0 cm^2 G/CNF and PANI-G/CNF films, respectively. Cyclic voltammetry and galvanostatic charging/discharging behavior were studied to evaluate the pseudocapacitive behavior and specific capacitance of the novel hierarchical porous electrodes, respectively. The microstructures and electrochemical performances of the G/CNF and PANI-G/CNF electrodes were discussed and compared. Consequently, the conclusions of the research were made.

2. Experimental

2.1. Materials

Polyacrylonitrile (PAN, Mw = 150,000) powder, *N,N*-dimethylformamide (DMF, 99%), ammonium persulfate (APS), sulfuric acid (H_2SO_4), and aniline monomer were purchased from Sigma–Aldrich Chemical Co. (St. Louis, MO, USA). Graphene nanosheets were supplied by XG Sciences, Inc. (Lansing, MI, USA). All the chemicals were used as received without further purification or modification.

2.2. Preparation of porous G/CNF and PANI-G/CNF films

The precursor graphene-beaded PAN (G/PAN) nanofibers with the diameter ~300 nm were prepared by electrospinning. During the process, PAN powder and graphene nanosheets (mass ratio 5:2) were first added into DMF to form an electrospinnable solution. The electrospinning process was performed in a high DC electrical field of 80 kV m^{-1}, which was generated by applying a 20 kV DC voltage to a 25 cm gap between the spinneret and the nanofiber collector. The graphene-beaded carbon nanofibers (G/CNFs) were yielded by consecutive stabilization, carbonization and activation of the electrospun precursor G/PAN nanofibers in a tubular quartz reaction furnace according to our recent synthesis route [22]. Subsequently, the yielded G/CNF films (~0.38 g) were coated with an ultrathin layer of thorn-like PANI nanorods to form ternary porous PANI-G/CNFs via *in situ* polymerization of aniline monomer in aqueous solution. During the process of polymerization, the as-prepared G/CNF mats had been first immersed into 200 mL aniline (0.03 M)/H_2SO_4 (1 M) aqueous solution in an ice bath (~0–5 °C) for 6 h. Then, APS dissolved in another 50 mL 1 M H_2SO_4 aqueous solution was slowly added dropwise into the mixture. The molar ratio of aniline/APS was adjusted to 4:1. The mixture had been continuously stirred for 12 h, and the color of the solution slowly changed into dark green. After polymerization, the resulting precipitates were filtered out and washed sequentially with deionized water and acetone. Finally, the wet product had been dried in a vacuum oven at 80 °C for 10 h. The areal mass density (mg cm^{-2}) of PANI-G/CNFs was calculated as ~1.5. The mass fraction of PANI in PANI-G/CNFs was ~52% based on the weight difference of the G/CNFs before and after polymerization.

2.3. Microstructural and electrochemical characterization

The surface morphology of as-prepared G/CNF and PANI-G/CNF mats was analyzed by using a high-resolution FE-SEM (JEOL JSM-7600F). Electrochemical characterization was performed using a two-electrode cell setup. 1 M H_2SO_4 aqueous solution and stainless steel wire meshes were utilized as the electrolyte and the current collector, respectively. The electrochemical performance of the supercapacitor cells was evaluated by cyclic voltammetry (CV), galvanostatic charge/discharge testing, and electrochemical impedance spectroscopy (EIS). The CV and galvanostatic charge/discharge curves were obtained by using a battery tester BT 2000

(Arbin Instruments, TX, USA), which were further used for evaluation of the capacitive behavior and calculation of the specific capacitance of the porous G/CNF and PANI- G/CNF electrodes, respectively. The CV response of the electrodes was determined at varying scan rate in the range from 5 to 50 mV s^{-1}. The galvanostatic charge/discharge testing was performed in the potential range of −0.2–0.8 V and at the current-density range from 0.15 to 15 A g^{-1}. A three-electrode electrochemical impedance spectroscopy (EIS) setup was employed for the electrochemical impedance measurements. A saturated calomel electrode was utilized as the reference electrode. The measurements were performed in the frequency range from 0.01 Hz to 100 kHz on an Electrochemical Multiplexer ECM8 (Gamry Instruments, Inc., PA).

3. Results and discussions

The surface morphologies and microstructures of the electrospun G/CNFs and PANI-G/CNFs were characterized by FE-SEM. Fig. 1 shows the typical SEM images of G/CNFs and PANI-G/CNFs at low and high resolutions, respectively. As shown in Fig. 1(A) and (B), G/CNFs apparently consist of two constituents, *i.e.,* carbonized nanofibers and unfolded, opened graphene nanosheets with porous structures. It can be observed that all the graphene nanosheets are firmly connected to the CNF segments at two ends. The graphene nanosheets could be connected to CNF segments via strong covalent C–C bonds, which can potentially enhance the electrical conductivity and specific surface area of the resulting G/CNF mat [22]. The graphene nanosheets are typically 6–8 nm in thickness and 1–5 micron in in-planar size, while the CNFs have an average diameter of 200–400 nm. Fig. 1(C) shows the SEM image of typical hierarchical nanostructure of PANI-G/CNFs, which were obtained via *in situ* polymerization of aniline monomer onto the G/CNFs in aqueous solution. It can also be observed from Fig. 1(C) that the dense thorn-like PANI nanorods were coated evenly onto the surfaces of both CNFs and graphene nanosheets. The diameter of the PANI nanorods is ~30–50 nm as estimated from the high-resolution SEM image as shown in Fig. 1(D). According to Kaner's mechanistic study [2], the diameter of PANI nanorods can be tailored by adjusting the concentration of aniline used in the polymerization process. In addition, the densely stacked PANI nanorods were interconnected each other to form a highly porous ultrathin surface layer, resulting in a high surface area and very efficient contact with the electrolyte solution. Serving as the supporting template for deposition of PANI nanorods, G/CNFs can also be exploited as the conductive filler and conductive channels for transport of electrons in supercapacitors. Therefore, such unique microstructure of G/CNFs was expected to enhance the electrochemical performance and mechanical stability of PANI-G/CNFs as used as porous electrodes in supercapacitors.

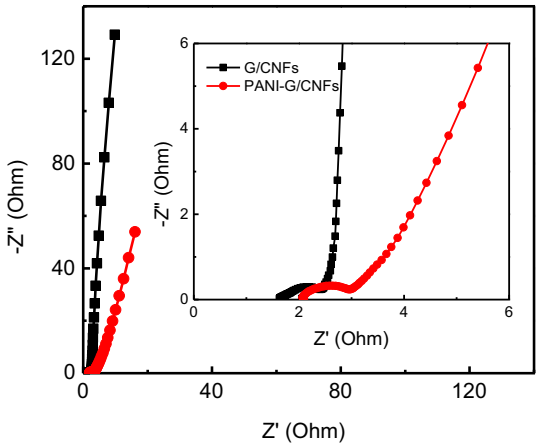

Fig. 2. Nyquist plots for G/CNF and PANI-G/CNF cells in 1 M H_2SO_4 solution in the frequency range from 0.01 Hz to 100 kHz. Z′ is the real part of the complex impedance; Z″ is the imaginary part of the complex impedance.

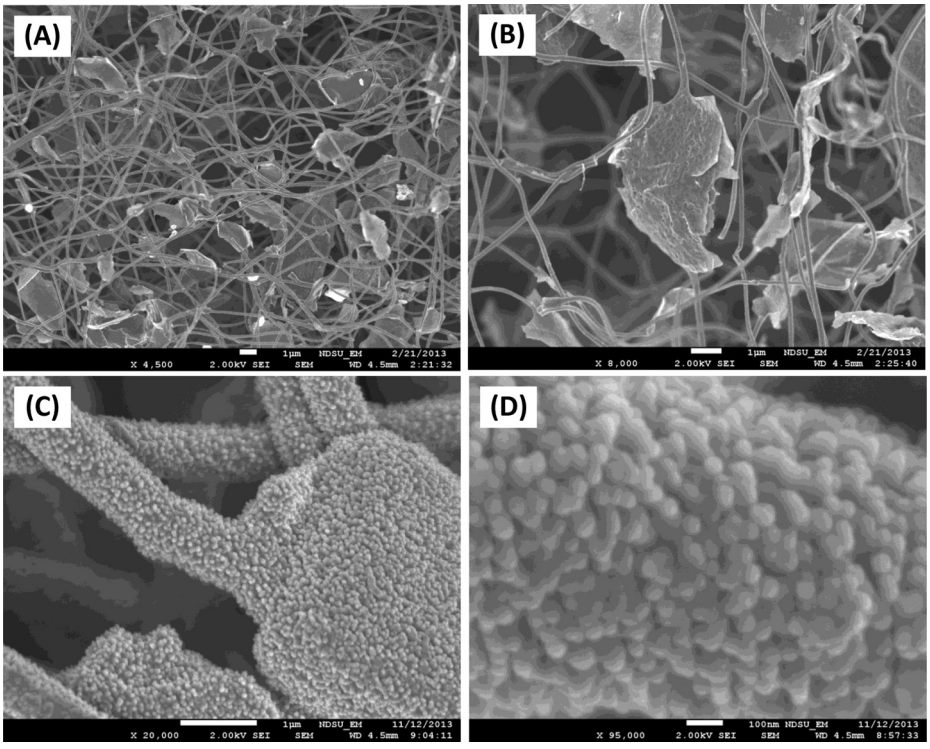

Fig. 1. SEM images of carbonized electrospun G/CNFs at low (A) and high (B) magnifications; SEM images of PANI-G/CNFs at low (C) and high (D) magnifications.

The electrochemical impedance of the porous G/CNFs and PANI-G/CNFs was measured by means of EIS method based on a three-electrode cell. EIS is a very effective method for characterization of the internal resistance, charge transfer in the electrode materials and electrolyte, and ion diffusion process of electrochemical devices. Fig. 2 shows the typical Nyquist plots of both G/CNF and PANI-G/CNF electrodes. The Nyquist plots consist of one incomplete semicircle and a nearly vertical line, which represent the charge transfer resistance of the electrode (R_{ct}) and the diffusion behavior of ions in the electrode pores, respectively [18,23]. As estimated from the intercept inFig. 2 insert, the equivalent series resistance (R_s) of G/CNF and PANI-G/CNF electrodes is ~1.6 and 2.0 Ω, respectively. In the mid- to low-frequency region, the vertical lines of G/CNF and PANI-G/CNF electrodes represent an ideal capacitive behavior with faster diffusion of ions in electrolyte. As calculated from the diameter of semicircles on the real axis inFig. 2 insert, the R_{ct} values of G/CNF and PANI-G/CNF electrodes are ~0.7 and 0.9 Ω, respectively. The R_{ct} resistance of PANI-G/CNF electrode is much less than the value reported for graphene nanosheets and PANI nanoworms (20.0 Ω) [24], PANI-nanorod/graphene composite (7.5 Ω) [4], and PANI/graphitized electrospun carbon fibers (2.4 Ω) [3]. The low R_{ct} resistance is attributed to the unique graphene-beaded nanostructures (Fig. 1(B)) and excellent electrical conductivity of G/CNFs.

The electrochemical performance of G/CNFs and PANI-G/CNFs was characterized by cyclic voltammetry (CV) and galvanostatic charge/discharge measurements based on a two-electrode supercapacitor cell. Fig. 3(A) shows the typical CV curves of G/CNFs, PANI-G/CNFs, and stainless steel mesh in the potential range from −0.2–0.8 V at a scan rate of 10 mV s^{-1}. The shape of CV curves of G/CNFs appeared in nearly rectangular shape and exhibited a rapid current response to voltage reversal, which occurred at each ending potential, indicating that G/CNFs had an excellent double-layer electrochemical capacitance. Different from the G/CNF electrodes, the CV curves of PANI-G/CNFs clearly exhibited two pairs of redox peaks (O_1/R_1 and Q_2/R_2), revealing the pseudocapacitive behavior of PANI. The peaks of O_1/R_1 are attributed to the reversible redox transition of PANI between the leucoemeraldine and polaronic emeraldine forms; whereas the peaks of O_2/R_2 represent the reversible Faradaic transformation of PANI between the emeraldine and pernigraniline forms [5,6,25]. Although a substantial quantity of PANI nanorods was coated onto G/CNFs, the nearly rectangle-shaped CV curves of PANI-G/CNFs indicated that the ternary porous PANI-G/CNFs had excellent electrochemical capacitive behavior [20].

Furthermore, the reversibility of redox reactions was determined by the potential difference between the oxidation and reduction peaks ΔE_{OR} [26]. The values of 0.11 and 0.18 V were obtained for ΔE_{O1R1} and ΔE_{O2R2} of PANI-G/CNFs, respectively. These values are lower than the values of 0.25 and 0.50 V for pure PANI fibers [19]. This observation indicates the high reversibility of PANI-G/CNF electrodes, which can be attributed to the low R_{ct} resistance. It is also noticed that the area formed by the CV loop and the current density of PANI-G/CNFs are both much larger than those of G/CNFs at the same scan rate, indicating a higher specific capacitance. The remarkable increases for the electrodes based on PANI-G/CNFs are obviously associated with doping PANI nanorods onto the surface of G/CNFs and the high electrical conductivity of G/CNFs. Fig. 3(B) shows the CV curves of the PANI-G/CNFs in 1 M H_2SO_4 aqueous solution at varying scan rate. As the scan rate increased from 5 to 50 mV s^{-1}, the cathodic peaks shifted to the right, while the anodic peaks shifted to the left. These shifts might be attributed to a slight increase of internal resistance at high scan rate [5,6,24]. At a high scan rate, once the electrolyte ions rapidly diffuse to the electrode, the response current will increase significantly. Furthermore, the current density response of PANI-G/CNFs increased obviously with increasing scan rate, which indicates a good rate capability of PANI-G/CNF electrodes.

In addition, galvanostatic charge–discharge plot (as shown in Fig. 4(A)) was used to determine the specific electrochemical capacitance of the above electrode materials at a constant current density of 0.3 A g^{-1} with a potential window of −0.2–0.8 V. It can be found from Fig. 4(A) that G/CNFs exhibited a nearly linear, symmetrical shape, which implies that the electrodes have an excellent electrochemical reversibility similar to ideal EDLCs. In contrast, PANI-G/CNFs behaved a slight deviation from linearity due to the Faradaic charge-transfer accompanied with the double-layer charging/discharging process. The voltage jump at the beginning of the discharge curve is related to the internal resistance (also called IR drop) of the electrode material. No obvious IR drops on the discharge curve of G/CNFs were measured, but a small IR drop was observed from the discharge plot of PANI-G/CNFs, indicating the low internal resistance of the capacitors as shown in Fig. 2. These results demonstrated that the unique porous G/CNF backbone networks effectively suppressed the internal electrical resistance of the PANI-G/CNF electrodes, resulting in improved electrochemical reversibility and charge-discharge efficiency compared to those of traditional graphene/PANI electrode materials [21–27]. The average specific capacitance value C_{avg} (F g^{-1}), of

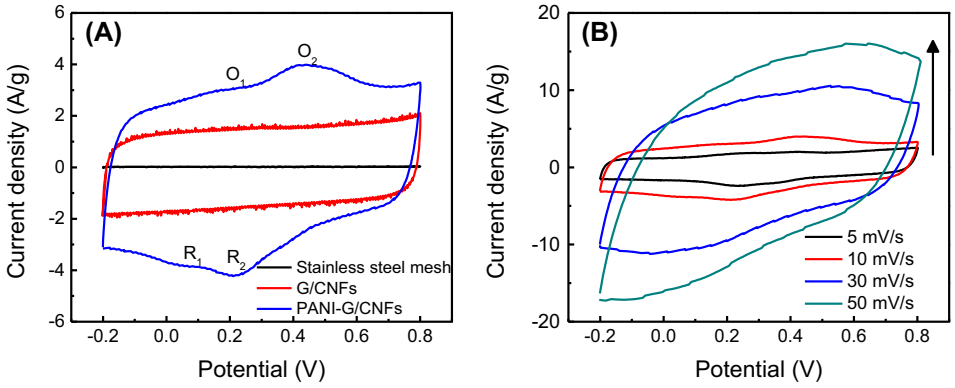

Fig. 3. (A) CV curves of G/CNFs, PANI-G/CNFs, and stainless steel mesh at a scan rate of 10 mV s^{-1} in 1 M H_2SO_4 aqueous solution in the potential range from −0.2–0.8 V; (B) CV curves of the PANI-G/CNFs at varying scan rate.

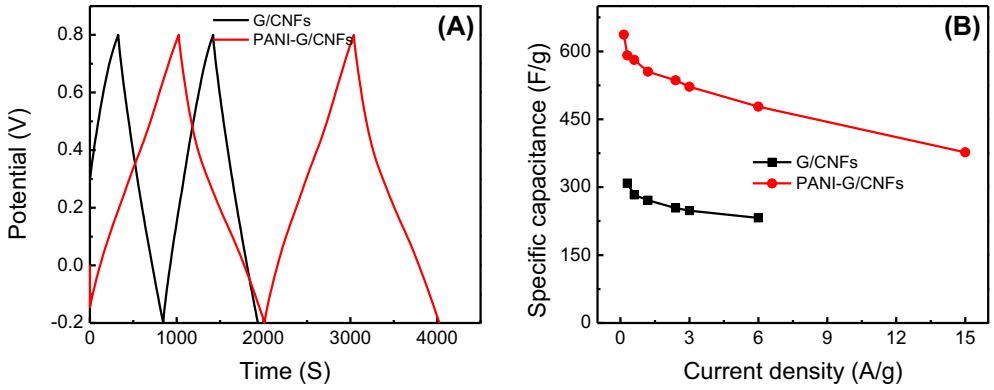

Fig. 4. (A) Galvanostatic charge-discharge curves of G/CNFs and PANI-G/CNFs at a constant current density of 0.3 A g^{-1}; (B) Specific capacitance of PANI-G/CNFs as a function of current density.

the resulting electrode materials can be calculated from the discharge process according to the formula:

$$C_{avg} = 2I\Delta t/(\Delta V m), \quad (1)$$

where I (ampere), m (gram), Δt (second) and ΔV (volt) represent the applied constant charge/discharge current, the mass of electrode material, the discharge time, and the potential difference (V) during the discharge process, respectively.

Based on the above formula, the experimental value C_{avg} of PANI-G/CNFs is as high as 591 F g^{-1} at a current density of 0.3 A g^{-1}, which is much higher than the value of 309 F g^{-1} for G/CNFs. Such a high value of pseudocapacitance of PANI-G/CNFs may be derived from the high theoretical value of pseudocapacitance (750 F g^{-1}) of PANI and the synergistic effect between thorn-like PANI nanorods and G/CNFs [15,28]. A high value of pseudocapacitance (520 F g^{-1}) of pure PANI film on Pt electrode has been measured by Yu et al. [29]. In the present study, 52 wt. % of PANI was coated onto the G/CNFs. Without taking into account the synergistic effect between PANI nanorods and G/CNFs, the theoretical value of specific capacitance of PANI-G/CNFs can be calculated as high as 419 F g^{-1} [309 F g^{-1} (G/CNFs) × 48 wt. % + 520 F g^{-1} (pure PANI) × 52 wt. %]. Thus, the value of specific capacitance increases by 172 F g^{-1} (591 F g^{-1}–419 F g^{-1}), up to 41% enhancement compared to the theoretical value of capacitance. Fig. 4(B) shows the variation of the specific capacitance of PANI-G/CNFs as a function of current density. It is noticed that the specific capacitance of PANI-G/CNFs decreases with increasing current density. The maximum value of specific capacitance of 637 F g^{-1} was obtained at a low current density of 0.15 A g^{-1}. In addition, PANI-G/CNFs could maintain a high value of specific capacitance of 478 F g^{-1} (only 25% decrease from 637 F g^{-1}) even at a high current density of 6 A g^{-1}. Furthermore, the value of capacitance of PANI-G/CNFs is larger than those of previously reported graphene/PANI electrodes [23–25,28]. The reason is that graphene-beaded CNF backbone networks not only contributed the charge pathway inside the PANI-G/CNFs, but also enhanced the specific surface area and electrical conductivity of the electrodes.

In all the electrochemical energy storage devices, energy and power densities are two major measures of their performance. Energy density is used to describe the amount of energy that can be stored per unit mass while power density is used to characterize how fast the energy can be stored or released. The energy density E_d (W h kg^{-1}) and power density P_d (W kg^{-1}) delivered by the electrodes of a supercapacitor are defined as [30]:

$$E_d = \frac{1}{2} C_s \Delta V^2, \quad (2)$$

$$P_d = \frac{E_d}{\Delta t}, \quad (3)$$

where C_s is the specific capacitance, ΔV is the voltage change of the supercapacitor between completely charged and discharged, and Δt is the discharge time. Fig. 5(A) is the Ragone plot of the supercapacitors with G/CNFs and PANI-G/CNFs as electrode materials, respectively. The maximum energy density of PANI-G/CNF-based supercapacitors is as high as 88 W h kg^{-1} at the power density of

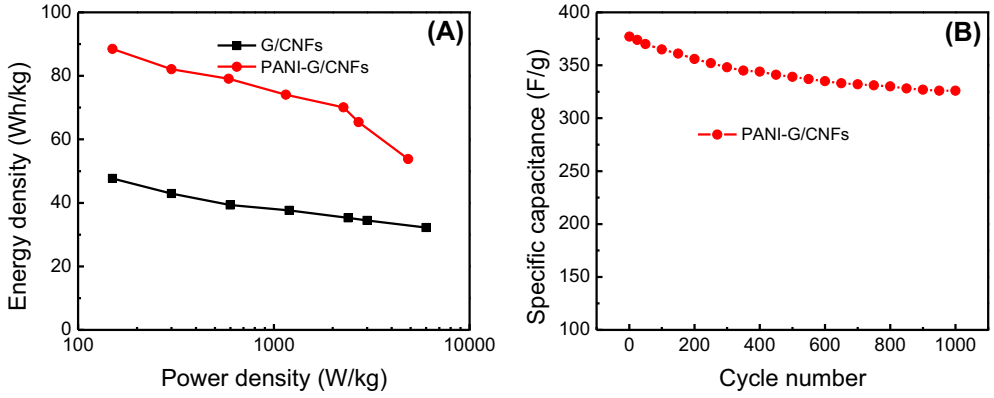

Fig. 5. (A) Ragone plots of G/CNF and PANI-G/CNF electrodes; (B) Cycle life tests of PANI-G/CNF electrodes measured at a constant current density of 15 A g^{-1}.

150 W kg^{-1}; the highest power density of G/CNFs is 6 kW kg^{-1} at the energy density of 32 W h kg^{-1}. The PANI-G/CNF based supercapacitors also kept an excellent rate capability, with the energy density of 54 W h kg^{-1} even at a high power density of 4.9 kW kg^{-1}. The measured power and energy densities of PANI-G/CNFs in this study are obviously higher than those of commercially available supercapacitors: 1–10 W h kg^{-1} and 1000–2000 W kg^{-1} [16]. Fig. 5(B) further shows the cycling performance of PANI-G/CNF based pseudosupercapacitors at the current density of 15 A g^{-1}. The value of capacitance only dropped ~13% from 377 to 327 F g^{-1} after 1000 cycles, competitive with the cycling stability of supercapacitors reported in the literature [5,21,29,30]. According to Fig. 2, the loss of specific capacitance of PANI-G/CNF based pseudosupercapacitors may be attributed to the increase of electrolyte solution resistance, the contact resistance between electrode and electrolyte, and the deterioration of ion diffusion [29].

4. Conclusions

In summary, a rational experimental route has been successfully formulated for synthesis of heterogeneous, porous PANI-G/CNFs for use as low-cost high-performance electrode materials for supercapacitors. Electrochemical characterization indicated that the novel nanofibrous electrode materials possessed the specific capacitance of 591 F g^{-1} at the current density of 0.3 A g^{-1} and the energy density of 54 W h kg^{-1} at the power density of 4.9 kW kg^{-1}. These experimental data indicate that PANI-G/CNFs exhibited excellent electrochemical performance for potential electrochemical energy storage. Specifically, the present PANI-G/CNFs can be used as low-cost, flexible, high-performance electrodes of supercapacitors without the need of conductive binders. Comparative study indicated that the excellent electrochemical performance of PANI-G/CNFs was resulted from the unique microstructures of the heterogeneous G/CNFs coated with ultrathin layers of thorn-like PANI nanorods. The G/CNFs provided a conductive network with high specific surface area, while the PANI nanorods further increased the specific surface area and triggered the excellent pseudocapacitive effect. The synergistic effect of the heterogeneous conductive G/CNF network backbones and pseudocapacitive PANI nanorods substantially enhanced the energy and power densities of the resulting nanofibrous electrode materials. In addition, synthesis of the present electrode materials only consists of three consecutive low-cost processes of electrospinning, controlled pyrolysis and *in situ* polymerization; therefore, manufacturing of the present high-performance electrode materials can be conveniently scaled up. This would greatly benefit the broader industrial applications of the present electrode materials for electrochemical energy storage devices.

Acknowledgment

The financial support of the research work by National Science Foundation (Award No.: CMMI-1234297), DOE EPSCoR Sustainable Energy Seed Grants Initiative (SUNRISE) (Award No.: DE-FG02-06ER46292), and ND EPSCoR Doctoral Dissertation Fellowship Award (Z. Zhou, 2013–2014) is gratefully acknowledged.

References

[1] K.S. Novoselov, A.K. Geim, S.V. Morozov, D. Jiang, Y. Zhang, S.V. Dubonos, I.V. Grigorieva, A.A. Firsov, Science 306 (2004) 666.
[2] J.X. Huang, R.B. Kaner, Angew. Chem. Int. Ed. 43 (2004) 5817.
[3] S.J. He, X.W. Hu, S.L. Chen, H. Hu, M. Hanif, H.Q. Hou, J. Mater. Chem. 22 (2012) 5114.
[4] L.W. Hu, J.G. Tu, S.Q. Jiao, J.G. Hou, H.G. Zhu, D.J. Fray, Phys. Chem. Chem. Phys. 14 (2012) 15656.
[5] W. Fan, C. Zhang, W.W. Tiju, K.P. Pramoda, C.B. He, T.X. Liu, ACS Appl. Mater. Interfaces 5 (2013) 3382.
[6] Y.G. Wang, H.Q. Li, Y.Y. Xia, Adv. Mater. 18 (2006) 2619.
[7] Z.-S. Wu, W.C. Ren, L.B. Gao, J.P. Zhao, Z.P. Chen, B.L. Liu, D.M. Tang, B. Yu, C.B. Jiang, H.-M. Cheng, ACS Nano 3 (2009) 411.
[8] Y.W. Zhu, S. Murali, M.D. Stoller, K.J. Ganesh, W.W. Cai, P.J. Ferreira, A. Pirkle, R.M. Wallace, K.A. Cychosz, M. Thommes, D. Su, E.A. Stach, R.S. Ruoff, Science 332 (2011) 1537.
[9] Y.B. Zhang, Y.W. Tan, H.L. Stormer, P. Kim, Nature 438 (2005) 201.
[10] M.H. Liang, L.J. Zhi, J. Mater. Chem. 19 (2009) 5857.
[11] J.D. Fowler, M.J. Allen, V.C. Tung, Y. Yang, R.B. Kaner, B.H. Weiller, ACS Nano 3 (2009) 301.
[12] Z.S. Wu, S. Pei, W. Ren, D. Tang, L. Gao, B. Liu, F. Li, C. Liu, H.M. Cheng, Adv. Mater. 21 (2009) 1756.
[13] Z.P. Zhou, X.-F. Wu, H. Fong, Appl. Phys. Lett. 100 (2012) 023115.
[14] R. Ruoof, Nat. Nanotechnol. 3 (2008) 10.
[15] K. Lota, V. Khomenko, E. Frackowiak, J. Phys. Chem. Solids 65 (2004) 295.
[16] X. Zhao, B.M. Sanchez, P.J. Dobson, P.S. Grant, Nanoscale 3 (2011) 839.
[17] H. Gomez, M.K. Ram, F. Alvi, P. Villalba, E. Stefanakos, A. .Kumar, J. Power Sources 196 (2011) 4102.
[18] K.S. Ryu, K.M. Kim, N.G. Park, Y.J. Park, S.H. Chang, J. Power Sources 103 (2002) 305.
[19] M.K. Liu, Y.-E. Miao, C. Zhang, W.W. Tjiu, Z.B. Yang, H.S. Peng, T.X. Liu, Nanoscale 5 (2013) 7312.
[20] S. Numao, K. Judai, J. Nishijo, K. Mizuuchi, N. Nishi, Carbon 47 (2009) 306.
[21] J. Yan, T. Wei, Z.G. Fan, W.Z. Qian, M.L. Zhang, X.D. Shen, F. Wei, J. Power Sources 195 (2010) 3041.
[22] Z.P. Zhou, X.-F. Wu, J. Power Sources 222 (2013) 410.
[23] L.F. Lai, H.P. Yang, L. Wang, B.K. Teh, J.Q. Zhong, H. Chou, L.W. Chen, W. Chen, Z.X. Shen, R.S. Ruoff, J.Y. Lin, ACS Nano 6 (2012) 5941.
[24] Y.S. Luo, D.Z. Kong, Y.L. Jia, J.S. Luo, Y. Lu, D.Y. Zhang, K.W. Qiu, C.M. Li, T. Yu, RSC Adv. 3 (2013) 5851.
[25] Z.F. Li, H.Y. Zhang, Q. Liu, L.L. Sun, L. Stanciu, J. Xie, ACS Appl. Mater. Interfaces 5 (2013) 2685.
[26] C.Y. Wang, V. Mottaghitalab, C.O. Too, G.M. Spinks, G.G. Wallace, J. Power Sources 163 (2007) 1153.
[27] P.A. Basnayaka, M.K. Ram, E.K. Stefanakos, A. Kumar, Electrochim. Acta 92 (2013) 376.
[28] N.A. Kumar, H.J. Choi, Y.R. Shin, D.W. Chang, L.M. Dai, J.B. Baek, ACS Nano 6 (2012) 1715.
[29] H.-P. Cong, X.-C. Ren, P. Wang, S.-H. Yu, Energy Environ. Sci. 6 (2013) 1185.
[30] Q. Cheng, J. Tang, N. Shinya, L.-C. Qin, J. Power Sources 241 (2013) 423.